JOURNAL OF SOLID STATE CHEMISTRY 137, 223–230 (1998)
ARTICLE NO. SC977708

Magnetic, Electrical Conductivity, and EPR Investigations of a Low-Spin d^5 System in $Fe_8V_{10}W_{16}O_{85}$

N. Guskos,[1] V. Likodimos, and S. K. Patapis

Solid State Section, Department of Physics, University of Athens, 15784 Zografos, Athens, Greece

J. Typek, M. Wabia, and H. Fuks

Institute of Physics, Technical University of Szczecin, 70-310 Szczecin, Poland

H. Gamari-Seale

National Center for Scientific Research "Demokritos," Aghia Paraskevi, Attikis, 15310 Athens, Greece

and

J. Walczak, I. Rychłowska-Himmel, and M. Bosacka

Department of Inorganic Chemistry, Technical University of Szczecin, 71-065 Szczecin, Poland

Received April 17, 1997; in revised form November 10, 1997; accepted November 14, 1997

The temperature dependence of the magnetic, electrical conductivity, and electron paramagnetic resonance (EPR) properties of $Fe_8V_{10}W_{16}O_{85}$ has been investigated. The magnetic susceptibility measurements revealed an almost Curie–Weiss law behavior above room temperature and an additional magnetic interaction at low temperature, causing a steep rise of magnetization as the liquid helium temperature was approached. The value of the magnetic moment at high temperature, $\mu_{eff} = 1.80\ \mu_B$, suggests a predominance of trivalent iron ions in a low-spin state. In the 300–4.2 K temperature range a difference between the zero field cooling (ZFC) and the field cooling (FC) modes was recorded. This irreversible behavior might be related to the presence of weakly coupled clusters. The EPR measurements revealed a broad, temperature-dependent resonance line at high temperature and two weaker lines at low temperature. The two low-temperature lines were attributed to antiferromagnetically coupled high-spin Fe^{3+} ion clusters and to high-spin iron ions placed at sites with low symmetry of the crystal field. The broad line at high temperature was separated into two Lorentzian lines. These component lines were attributed to the two paramagnetic centers connected with the Fe^{3+} ions involved in the magnetic structure of $Fe_8V_{10}W_{16}O_{85}$: dominant low-spin centers and a small admixture (<15%) of the high-spin centers. The line broadening and shift of the resonance field of the two component lines with decreasing temperature were studied and analyzed using a model of the EPR lines of antiferromagnets. The temperature dependence of the electrical conductivity showed a typical semiconducting-type behavior with an activation energy of 0.40 eV. The hopping mechanism of small polarons was proposed to explain the transport properties of the sample. © 1998 Academic Press

[1]To whom correspondence should be addressed.

INTRODUCTION

Three-component systems of transition metal oxides such as Fe_2O_3–V_2O_5–MoO_3, Cr_2O_3–V_2O_5–MoO_3, Al_2O_3–V_2O_5–MoO_3, and Fe_2O_3–V_2O_5–WO_3 have been the subject of many investigations not only because they are scientifically interesting but also because they have application in catalytic devices. The last system seemed to be the least investigated and therefore attracted our attention (1). As with other three-component systems, Fe_2O_3–V_2O_5–WO_3 is built from three binary systems, i.e., Fe_2O_3–V_2O_5, V_2O_5–WO_3, and Fe_2O_3–WO_3. In the first binary system, two compounds exist: $FeVO_4$ and $Fe_2V_4O_{13}$ (2), which are *n*-type antiferromagnetic semiconductors (3). In the V_2O_5–WO_3, one compound, namely Fe_2WO_6, appearing in three polymorphic forms was identified (4). Magnetic susceptibility and EPR measurements at low temperature revealed a significant paramagnetic contribution, probably resulting from local distortions of the antiferromagnetic bulk structure induced by a disturbed cation ordering or the presence of Fe^{2+} ions (5). The EPR spectra of α, β, and γ-Fe_2WO_6 exhibited the presence of various paramagnetic iron centers,

0022-4596/98 $25.00

which were tentatively attributed to the existence of two kinds of isolated trivalent iron ions in a moderate and weak crystal field of low symmetry, respectively, and to the formation of iron clusters producing ground states with $S = \frac{1}{2}$ and $S = \frac{3}{2}$ (5). Moreover, EPR investigation of $FeVO_4$, α, β, and γ-Fe_2WO_6, and $Fe_2V_4O_{13}$ in the 300–5 K temperature range revealed a broad resonance line that changes strongly during the phase transition to the magnetic ordering state (3, 5, 6).

Recently, a new phase in the Fe_2O_3–V_2O_5–WO_3 system was identified (7) in which formation of all three oxides is involved. This new phase can be described by the molecular formula $Fe_8V_{10}W_{16}O_{85}$. To date, very little is known about the physical properties of this compound. In the present work the temperature dependence of the magnetic susceptibility, conductivity, and EPR spectra of $Fe_8V_{10}W_{16}O_{85}$ is reported for a wide range of temperatures.

EXPERIMENTAL

The $Fe_8V_{10}W_{16}O_{85}$ samples used in our measurements were prepared by the solid state reaction technique. The composition of the initial mixture in terms of oxide content was as follows 16.00 mol% α-Fe_2O_3, pure for analysis (p.a.), recalcined at 1000°C for 24 h three times; 20.00 mol% V_2O_5, p.a.; 64.00 mol% WO_3, p.a., recalcined at 700°C for 24 h. The final product was obtained by mixing $FeVO_4$, WO_3, and V_2O_5. The $FeVO_4$ phase was obtained by the method given in ref 2. The following heating process was applied: 600°C for 24 h, 620°C for 48 and 72 h, 700°C for 48 h, 720°C for 48 h, 720°C for 6 h (two times), 725°C for 3 h (four times), 735°C for 3 h. The synthesis reaction could be written as $8FeVO_4 + V_2O_5 + 16WO_3 \rightarrow Fe_8V_{10}W_{16}O_{85}$.

Identification of the samples was made on a Dron-3 X-ray powder diffractometer using Co$K\alpha$ radiation and an iron filter. Only one major phase was observed, showing rhombic symmetry and the following unit cell parameters: $a = 7.5631(12)$, $b = 18.0227(33)$, and $c = 21.7851(44)$ Å. The volume of the unit cell is 2969.47 Å^3. The experimental value of density is $\rho = 5.94(5)$ g/cm^3 and is in reasonable agreement with the Roentgen density ($\rho = 5.88(2)$ g/cm^3). Differential thermal analysis (DTA) was also used to confirm the existence of the new phase. A symmetrical endothermic DTA peak, starting at 830 ± 5°C and attributed to the melting point of the investigated phase (7), was registered only for samples obtained from the initial mixture $8FeVO_4 + V_2O_5 + 16WO_3$.

The EPR measurements were carried out using a standard X-band ($\nu = 9.118$ GHz) spectrometer of the Radiopan R-10 type with 100-kHz magnetic field modulation. The measurements were performed on an Oxford helium flow cryostat system in the 4.2–290 K temperature range. The magnetic field induction was monitored using a digital proton magnetometer, whereas the microwave frequency was controlled by using a high-Q wavemeter. The sample weighed about 30 mg and was placed in a quartz tube with a diameter of 2 mm in flowing He gas to avoid oxygen condensation.

Magnetic susceptibility measurements were performed on closely packed powder samples using a PAR 155 vibrating sample magnetometer at low temperatures and a magnetic balance above room temperature. The measurements were done in the temperature range from 4.2 to 900 K in a magnetic field of 0.02 or 0.5 T.

The electrical conductivity of the samples was measured using the dc four-point technique. Contact of the four leads was achieved through a silver point. The sample was fed by a current source (Keithley 224) with a current of 1 mA, which corresponds to a current density of about 0.02 A/cm^2. The voltage was measured with a Keithley 181 nanovoltmeter.

RESULTS AND DISCUSSION

Magnetic Susceptibility Measurements

The temperature dependence of the inverse susceptibility of $Fe_8V_{10}W_{16}O_{85}$ at low and high temperatures is shown in Fig. 1. The observed behavior can be separated into three regions: a high-temperature region above 300 K, a low-temperature region below 30 K, and an intermediate region between 30 and 300 K. At high temperatures the χ^{-1} vs T curve exhibits an almost linear dependence (Fig. 1a), which can be described by a Curie–Weiss law, $\chi = C/(T - \theta)$, with a Curie–Weiss constant $\theta = 120$ K, suggesting the presence of ferromagnetic interactions in our compound. If it is assumed that only the iron ions are paramagnetic, an effective magnetic moment of $\mu_{\text{eff}} \approx 1.80\ \mu_B$ can be calculated from the obtained C constant. Below room temperature, in the intermediate region, the susceptibility deviates from a simple Curie–Weiss law, and, moreover, differences between the FC and ZFC modes were recorded in the temperature range 250–4 K, taken at a field 20 mT (Fig. 1a). The sample was cooled to liquid helium temperature and then warmed to room temperature. Although the character of the susceptibility curves for FC and ZFC was almost the same, the actual values of the susceptibility at the same temperature were different for the processes. Below 30 K, in the low-temperature region, a steep rise of magnetic susceptibility with decreasing temperature was recorded. During the FC process a maximum of susceptibility was recorded at 6 K, but this maximum was not observed for the ZFC process. The ZFC and FC were irreversible processes and could be related to the presence of weakly coupled clusters which, after being thermally treated under the applied magnetic field, become decoupled from the magnetic ordering background, giving rise to an enhanced paramagnetic contribution.

The supposition that we have to deal with V^{4+} and W^{5+} does not explain the temperature dependence of the

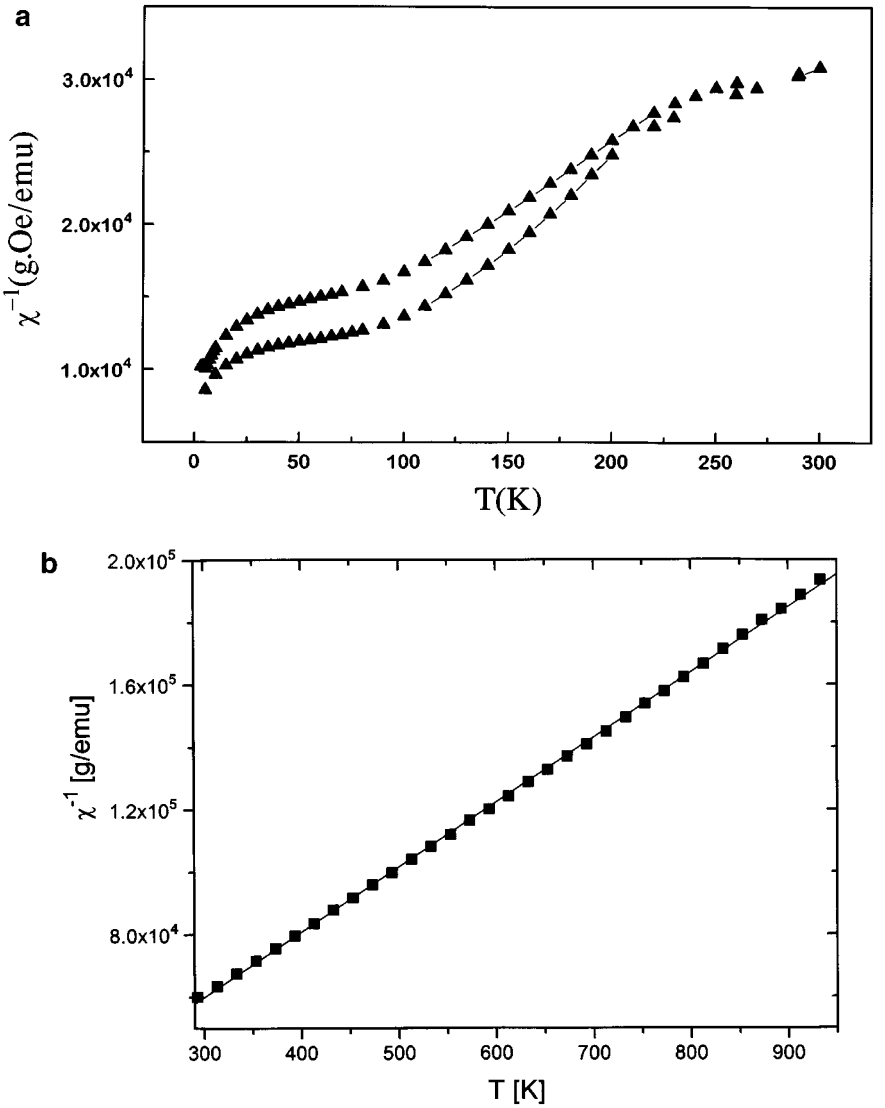

FIG. 1. Temperature dependence of the inverse susceptibility of $Fe_8V_{10}W_{16}O_{85}$: (a) below room temperature, in the ZFC and FC modes; (b) above room temperature.

magnetic susceptibility. A possible explanation is that the iron ions are in a low-spin state. At high temperature the paramagnetic centers, which do not take part in the magnetic ordering at low temperature, are dominant. Taking this into account, the observed Curie–Weiss law could be explained. Assuming that the obtained magnetic susceptibility may be written as a sum of three independent susceptibilities, $\chi(\text{obs}) = \chi_{\text{Fe}}(\text{high spin}) + \chi_{\text{Fe}}(\text{low spin}) + \chi_{\text{W}}$, one can estimate that only about 15% of the total susceptibility is due to the high-spin trivalent iron ions. On the other hand, the number of iron atoms in $Fe_8V_{10}W_{16}O_{85}$ that could be expected to carry uncompensated spins depends on the existing chemical bonding in the crystal structure (8). Because the positions of the atoms in the unit cell are not known, one can only speculate that if, on average, only 2.4 iron atoms in the formula unit were magnetic and in a high-spin state, that situation could also explain the observed value of the magnetic moment.

Figure 2 presents the temperature dependence of the effective magnetic moment μ_{eff} at high temperature, where μ_{eff} is defined as $\mu_{\text{eff}} = 2.828(\chi T)^{1/2}$ and χ has units of emu/mole. As can be seen, the value of μ_{eff} reaches a maximum around $T_{\max} \sim 450$ K and then decreases with increasing temperature. The expected smaller value of μ_{eff} for the iron ion as well as the high value of $T_{\max}$ suggests the existence of an antiferromagnetic intercluster interaction. It is known that a plot of μ_{eff} vs T does not exhibit a maximum if a simple Heisenberg exchange process with isotropic

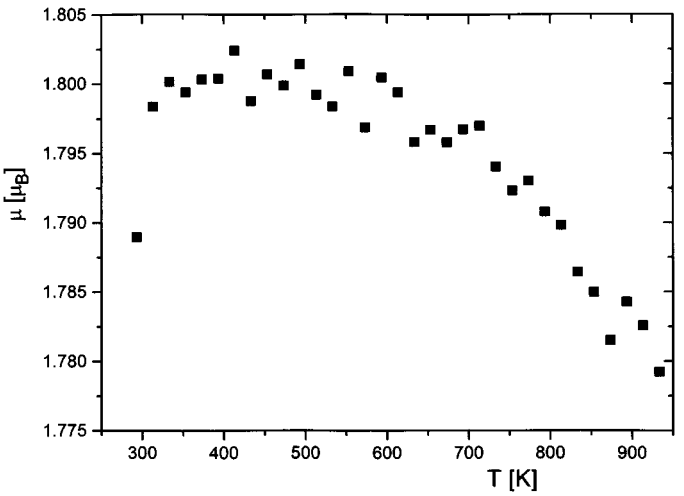

FIG. 2. Temperature dependence of the calculated effective magnetic moment μ_{eff} at high temperature.

exchange interaction is assumed. By allowing for an antiferromagnetic interaction, the μ_{eff} vs T plot passes through a maximum. The corresponding curve in Fig. 2 indicates that these interactions are operative over a wide temperature range and not only below $T_{\max}$, where they become dominant.

Electron Paramagnetic Resonance

Figures 3 and 4 present the EPR spectra of $Fe_8V_{10}W_{16}O_{85}$ in different temperature ranges. Figure 3 shows the EPR spectrum at 4.2 K, the lowest temperature of measurement, and Figure 4 presents an overview of the spectra at higher temperatures. At 4.2 K the EPR spectrum consists of only two lines of different intensity. The more intense line with the Gaussian lineshape is centered at $g_{\text{eff}} = 1.979(3)$ and has a linewidth $\Delta H = 52.0(1)$ mT. Its g value and linewidth do not show any temperature variation. The intensity of this line decreases with increasing temperature. The spectrum resembles the EPR line usually observed for an $S = \frac{1}{2}$ spin system. The $S = \frac{1}{2}$ spin state might arise in our case from the antiferromagnetic coupling of one high-spin Fe^{3+} ($S = \frac{5}{2}$) with one Fe^{2+} ($S = 2$) ion as reported for [2Fe–2S]ferrodoxin (9) or, more likely, from a cluster of three antiferromagnetically coupled high-spin Fe^{3+} ions. If the three exchange coupling constants are similar in value, then the state with $S = \frac{1}{2}$ becomes the ground state of the cluster (5). In our case the observed EPR line has disappeared at a temperature of about 30 K.

The other, less intense low-temperature line is centered at $g_{\text{eff}} = 4.097(2)$ and has a linewidth $\Delta H = 18.9(1)$ mT at 4.2 K. The parameters of this line vary with temperature: the value of the g factor and its linewidth decrease with increasing temperature. The temperature dependence of the linewidth ΔB can be satisfactorily described by the following equation: $\Delta B(T) = \Delta B(\infty)(1 + \Theta/T)$, with $\Delta B(\infty) = 4.54$ mT and $\Theta = 12.8$ K. On the other hand, the g factor decreases linearly with temperature, according to the formula $g(T) = g(0) - aT$, with $g(0) = 4.14$ and $a = 0.010\ \text{K}^{-1}$. The low-field EPR line is characteristic of high-spin Fe^{3+} ions in a strong crystal field with an extreme rhombic distortion. The theory of large g values

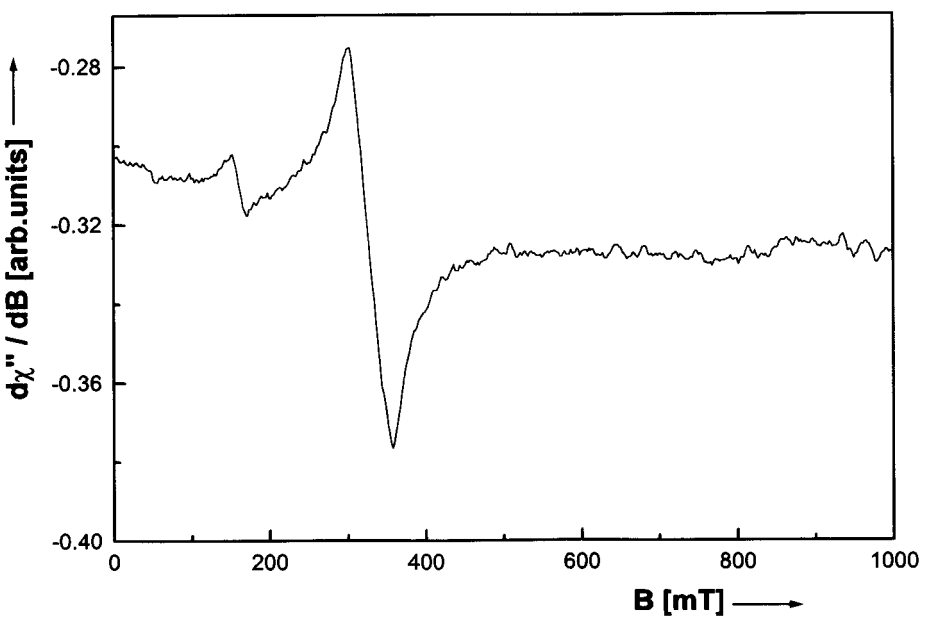

FIG. 3. EPR spectrum of $Fe_8V_{10}W_{16}O_{85}$ at 4.2 K.

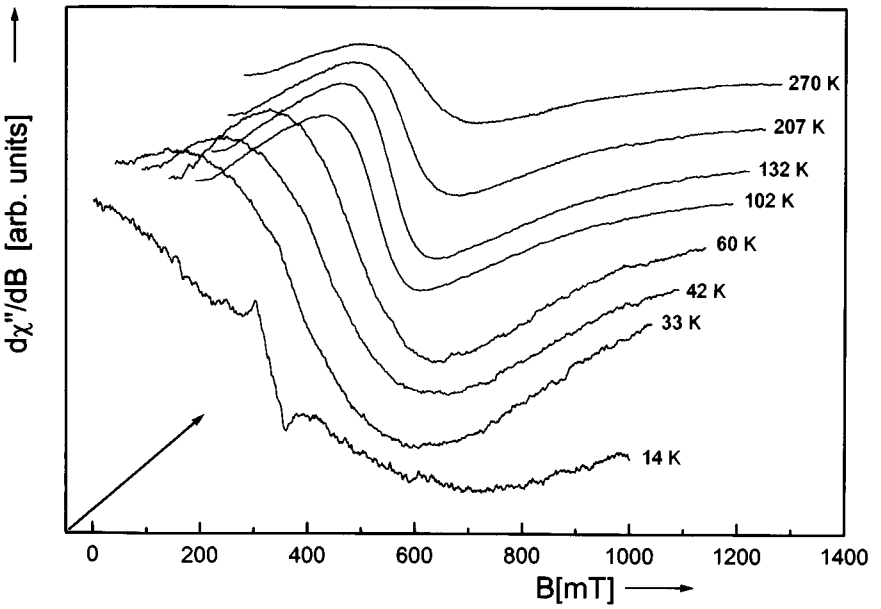

FIG. 4. Overview of EPR spectra taken at different temperatures. The magnetic field axis is appropriate only for the spectrum at the lowest temperature.

for a high-spin ground state Fe^{3+} is based on the spin Hamiltonian:

$$H = \beta S \cdot \mathbf{g} B + D(S_z^2 - S(S+1)/3) + E(S_x^2 - S_y^2), \quad [1]$$

where β is the Bohr magneton, S is the effective spin, and $\mathbf{g}$ is a second-rank tensor with the eigenvalues g_x, g_y, and g_x. D $(=B_2^0)$ and E $(=B_2^2)$ are the axial and orthorhombic components that describe the splitting of the Fe^{3+} Kramers doublets in the crystal field. The orthorhombic character of the field is expressed by the ratio $E/D = \lambda$. $\lambda = 0$ implies a crystal field of axial symmetry, and $\lambda = \frac{1}{3}$ corresponds to a completely rhombic field. A single EPR signal at $g_x = g_y = g_z = 4.27$ will be observed when $\lambda = \frac{1}{3}$ and $hv/D < 1$. Values of g as a function of λ were calculated by Gaite and Michoulier (10). The observed shift of g with temperature toward lower values for our compound could then be explained as a decrease of orthorhombicity of the crystal field. A similar behavior was observed for Fe^{3+} centers in cristobalite and tridymite (11). In our case, λ changed form 0.32 to 0.28 with increasing temperature. Another possible explanation for the temperature change of the g parameter and the linewidth involves the dynamical spin fluctuation existing before the phase transition to the magnetic ordered state, such as that seen in the magnetic susceptibility behavior at helium temperatures.

Both of these low-temperature lines disappear completely above 30 K, and the EPR spectrum of $Fe_8V_{10}W_{16}O_{85}$ is dominated by a very broad line with a strongly temperature-dependent resonance field and linewidth. Since the values of the resonance field and the linewidth are comparable, both positive and negative components of the dynamic susceptibility have been taken into account in considering the absorbed microwave power. The analysis of the lineshape of the high-temperature line revealed that it could not be approximated by a single Lorentzian or Gaussian curve at all investigated temperatures, but the observed lineshape can be satisfactorily explained by the sum of two Lorentzian curves having different amplitudes, resonance fields, and linewidths (Fig. 5). This indicates that we have to deal with two different iron sites, although one dominates at all investigated temperatures. A similar situation is often encountered. The observed EPR line of Fe^{3+} ions in $Fe_2V_4O_{13}$ is slightly asymmetric, which is the result of the fact that iron ions in the lattice occupy at least two nonequivalent positions (3). In $Fe_2V_4O_{13}$, within the limits of experimental error, there are no changes in the g value induced by temperature whereas there is a very strong temperature dependence of the linewidth (3). For $FeVO_4$, both resonance field and linewidth depend on temperature (6). As the broad line was separated into two lines, one narrow (designated component 1) and one broad (designated component 2), further analysis will be done for each line separately. The magnetic center connected with component 2 contains the majority of spins, and although that percentage seems to change only very slightly with temperature, it is never below 85% of the total number of spins. The integral intensity I, defined as $I = bA(\Delta B)^2$, where b is the proportionality factor, A is the EPR signal amplitude, and ΔB is the peak-to-peak linewidth, has shown the same

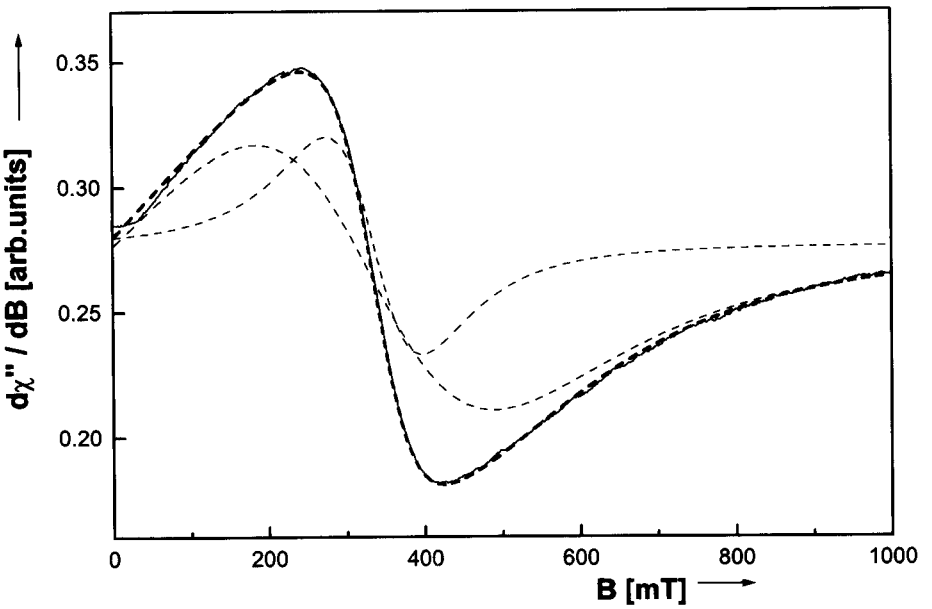

FIG. 5. Decomposition of the EPR spectrum at 102 K into two (– – –) Lorentzian lines; (· · ·) experimental line, (——) sum of two simulated lines.

paramagnetic-type temperature dependence for both components. In Fig. 6 this dependence is shown for the more intense component 2. The temperature dependence of the effective g factor for the components is different. For the center 1, the g factor increases linearly with increasing temperature, and the change can be described by the formula $g(T) = 1.928 + 0.0003T$ [K]. For the center 2, the g factor is fairly constant from room temperature to 70 K, having a value of 1.975. Below 70 K, a sharp decrease to a value of 1.900 at 30 K is observed.

The broadening of the EPR linewidth ΔB with decreasing temperature was detected for both component lines (Fig. 7),

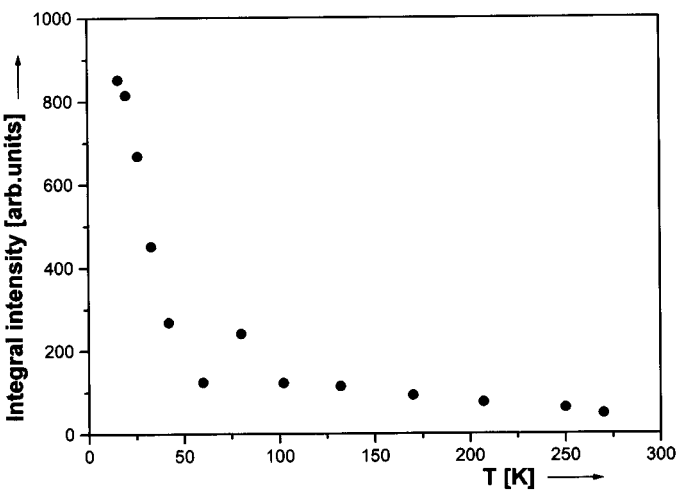

FIG. 6. Temperature dependence of total intensity for component 2 of the broad line.

and also the form of that dependence was the same. For both components, the linewidth followed a simple T^{-1} dependence; thus it can be described by the equation

$$\Delta B(T) = \Delta B(\infty)(1 - \Theta/T), \qquad [2]$$

with $\Delta B(\infty) = 81$ mT and $\Theta = -83$ K for component 1 and $\Delta B(\infty) = 240$ mT and $\Theta = -47$ K for component 2. The divergent behavior of the EPR linewidth ΔB in exchange-coupled paramagnets is often observed as the critical temperature T_N is approached from above. It is well established that for uniaxial antiferromagnets the EPR line broadens as $T \to T_N$ from the high-temperature region and narrows for cubic antiferromagnets (12). That ΔB continues to decrease with increasing temperature also in a region extending over the critical region, that is, for $T > 3T_N$, was observed and explained by Dorman and Jaccarino (13). They obtained the same expression (2) for the temperature dependence of the EPR linewidth.

Concerning the origin of these two component lines, we think that the center 1 is connected with high-spin Fe^{3+} ions in an axial field, while the more abundant center 2 is produced by low-spin ferric ions in an axial crystal field with a strong rhombic distortion. This assumption makes magnetic susceptibility and EPR measurements consistent. A review of the EPR spectra of low-spin ferric ions in crystal fields of different axial and rhombic distortions has been published by Harris (9). The g parameter and the effective magnetic moment μ_{eff} values as a function of tetragonal and rhombic distortions have been calculated. Diagonal and off-diagonal matrix elements have been given in terms of

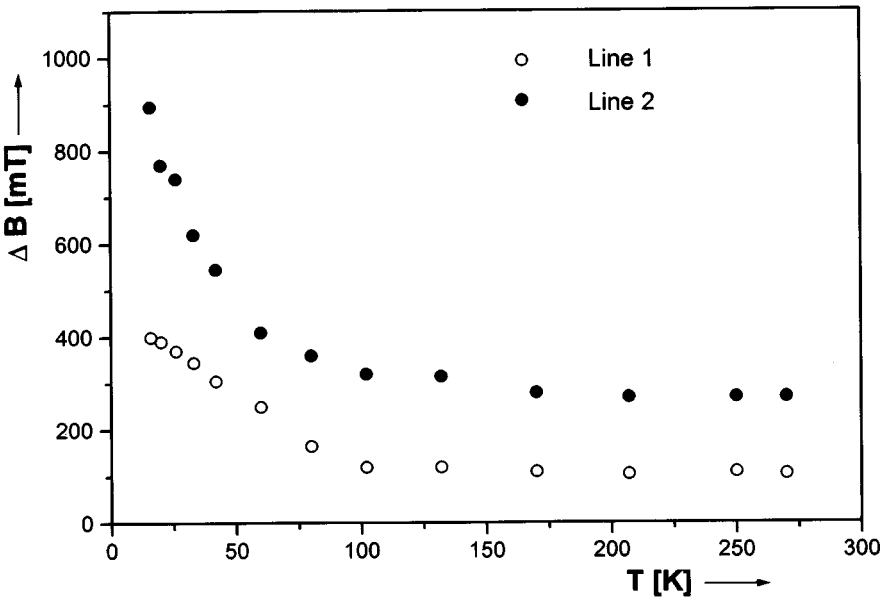

FIG. 7. Temperature dependence of the peak-to-peak linewidth for component 1 (open circles) and component (filled circles) of the broad line.

two crystal field parameters, μ (a measure of the difference in bonding perturbation of the four in-plane ligands and the two axial ligands along the z axis) and R (a measure of the rhombic distortion). For $R/\mu = 2$ and $\delta/\mu = 0.01$, where δ is the spin–orbit coupling parameter, the following values of the spin-Hamiltonian parameter g_{eff} and the magnetic moment have been obtained: $g_{\text{eff}} = 2.003$ and $\mu_{\text{eff}} = 1.74\,\mu_{\text{B}}$. This case of μ and R corresponds to a strong axial crystal field with a large rhombic distortion. The calculated values are in very good agreement with what we obtained for our compound. The six $^2T_2$ states are all degenerate in an octahedral symmetry and interact among themselves under the influence of the spin–orbit coupling, and there is a tetragonal and rhombic distortion of the local perturbing environment as well. As can be seen, the rhombic distortion is strong with weaker spin–orbit coupling. Usually this EPR line is observed only at lower temperatures.

Additional EPR lines centered at $g_{\text{eff}} = 1.051(5)$ are observed at 15 K. These lines may possibly originate from W^{5+} ions. The W^{5+} ion has one $5d$ electron outside the closed shell. Thus only one resonance line could be observed with the effective spin $\frac{1}{2}$, corresponding to a valence state $5+$. The lines observed for our compound may arise from isolated W^{5+} ions with a hyperfine structure (14, 15). The g parameter for a free electron has the value of 2.0023, but for ions situated inside a compound it may be changed by $\Delta g_{ii} = -2\lambda \sum_j |\langle 0|L_i|j\rangle|^2/(E_j - E_0)$, where λ is the spin–orbit coupling, E_0 is the energy of the ground state, and E_j is the energy of the higher states determined by the crystalline field. Furthermore, the effect of covalency would be to reduce the effective value of λ.

Conductivity Measurements

The electrical resistivity curve for the sample follows a semiconducting-type behavior. Figure 8 presents plots of $\ln\sigma$ (σ is the dc electrical conductivity) vs T^{-1} in the temperature range 100–400 K. The temperature dependence of the conductivity σ could be described in the entire investigated temperature range by the following well-known exponential relation:

$$\sigma(T) = \sigma \exp(-E/kT), \qquad [3]$$

where σ is a constant, E is the activation energy, and k is the Boltzmann constant. The numerical values of these parameters for our sample are $E = 0.40$ eV and $\sigma = 4.0\,\Omega^{-1}\,\text{m}^{-1}$. The antiferromagnetic system Fe_2O_3–V_2O_3 doped with MoO_3 has shown a similar character of conductivity (3). Electronic conduction in solid oxides can occur by motion of charge carriers in a band or by a diffusion-like motion, called the hopping mechanism. The hopping mechanism applies to low-mobility oxide semiconductors at elevated temperatures and the charge carrier is called a small polaron. The value of the activation energy seems to be too low to be the activation energy for intrinsic conduction; therefore we assume that the conduction is of the extrinsic type. This type of conduction exists when mixed valence states of iron are present in the compound (16). The increase of electrical conductivity with increasing temperature is caused by the increase in the mobility of charge carriers. In $3d$ transition-metal oxides there is the possibility of small polaron formation. Since small polaron band

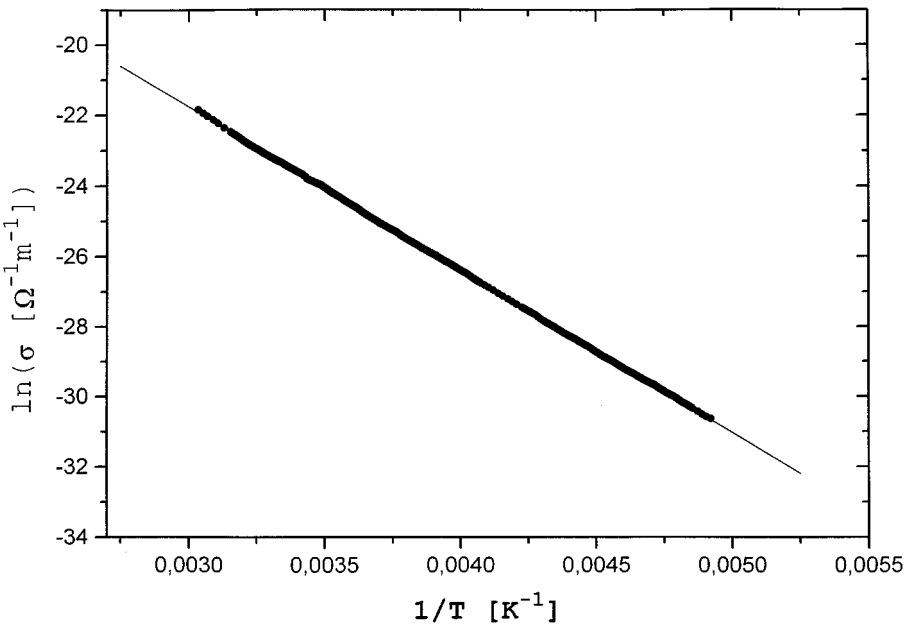

FIG. 8. $\ln\sigma$ vs T^{-1} in the 100–400 K temperature range for $Fe_8V_{10}W_{16}O_{85}$.

conduction is not possible at high temperatures (17), the hopping mechanism seems probable. In this mechanism a small polaron migrates from one lattice site to an adjacent site with a thermal activation energy of 0.40 eV.

CONCLUSIONS

Magnetic susceptibility measurements have shown the Curie–Weiss law behavior, with a predominance of low-spin-state iron ions at higher temperatures. Between 300 and 4.2 K differences between the FC and ZFC modes were registered. The EPR spectra exhibited the presence of various paramagnetic iron and tungsten centers. The low-temperature EPR spectra were tentatively attributed to the existence of two kinds of isolated Fe^{3+} centers, one in the high-spin state in a strong orthorhombic crystal field of decreasing orthorhombicity with increasing temperature, and the other with clusters of three antiferromagnetically coupled high-spin iron ions. Also the lines from W^{5+} ions were observed at low temperatures. In the high-temperature region a broad EPR line was observed. This line was assumed to be a superposition of two lines arising from two different centers of iron ions. The temperature behavior of the linewidth and g parameter for these two centers was investigated and described by a model of the EPR lines of antiferromagnets. However, to have a more complete picture of the magnetic behavior of this system, it would be convenient to measure the Mössbauer and neutron diffraction spectra. The strong interaction of crystal field could influence the spin states and conductivity properties.

ACKNOWLEDGMENT

We thank Mr. B. Bojanowski from the Institute of Physics, Technical University of Szczecin, for help in the experimental EPR work.

REFERENCES

1. J. Walczak and I. Rychlowska-Himmel, *J. Therm. Anal.* **36,** 2161 (1990).
2. J. Walczak, J. Ziolkowska, M. Kurzawa, J. Osten-Sacken, and M. Lysio, *Pol. J. Chem.* **59,** 255 (1985).
3. J. Kuriata, L. Sadlowski, B. Bojanowski, J. Walczak, M. Kurzawa, and J. Pichet, *J. Mater. Sci. Lett.* **7,** 144 (1988).
4. J. Walczak, I. Rychlowska-Himmel, and P. Tabero, *J. Mater. Sci.* **27,** 3680 (1992).
5. N. Guskos, L. Sadlowski, J. Typek, V. Likodimos, H. Gamari-Seale, B. Bojanowski, M. Wabia, J. Walczak, and I. Rychlowska-Himmel, *J. Solid State Chem.* **120,** 216 (1995).
6. B. Bojanowski, J. Kuriata, and L. Sadlowski, *Mol. Phys. Rep.* **5,** 138 (1994).
7. J. Walczak and I. Rychlowska-Himmel, *J. Mater. Sci.* **29,** 2745 (1994).
8. M. E. Danebrok, C. B. H. Evers, and W. Jietschko, *J. Phys. Chem. Solids* **57,** 381 (1996).
9. G. M. Harris, *Biophys. J.* **10,** 196 (1970).
10. J. M. Gaite and J. Michoulier, *Bull. Soc. Miner. Crystallogr.* **93,** 341 (1970).
11. H. Rager and H. Schneider, *Am. Mineral.* **71,** 105 (1986).
12. D. L. Huber, *Phys. Rev. B* **6,** 3180 (1972).
13. E. Dorman and V. Jaccarino, *Phys. Lett. A* **48,** 81 (1974).
14. T. T. Chang, *Phys. Rev.* **147,** 264 (1966).
15. A. Watterich, O. R. Gilliam, L. A. Kappers, and K. Raksanyi, *Solid State Commun.* **97,** 477 (1996).
16. S. Gupta, Y. P. Yadava, and R. A. Singh, *J. Mater. Sci. Lett.* **5,** 736 (1986).
17. I. K. Naik and T. Y. Tien, *J. Phys. Chem. Solids* **39,** 311 (1978).